Macromolecular Symposia

www.ms-journal.de

Hierarchical Nanotube Self-Assembly of DNA Minor Groove-Binding Ligand DB921 via Alkali Halide Triggering

Ryo Mizuta, Juliette M. Devos, Theyencheri Narayanan, Mizar Oliva, Melissa Gray, Jessica Webster, Wai-Li Ling, Adam Round, Deeksha Munnur, Estelle Mossou, Abdelbasset Farahat, David W. Boykin, W. David Wilson, Stephen Neidle, Ralf Schweins, Patrice Rannou, Michael Haertlein, V. Trevor Forsyth, and Edward Mitchell**

A systematic study into a novel self-assembling system is presented whereby the small molecule DB921 forms nearly monodisperse nanotubes upon addition of a suitable salt. Small-angle X-ray scattering and negative stain transmission electron microscopy are employed as the principal characterization methods to study both the fundamental assembly processes and reaction kinetics. The assembly is found to be hierarchical, culminating with helical winding of intermediate ribbon structures into nanotubes. The driving force for this process is likely the electrostatic interaction between DB921 and salt anions; this aspect can be used to control nanotube assembly and morphology.

1. Introduction

Self-assembling systems consist of materials that enable complex structures to form from molecular building blocks without external impetus. In particular, the chemical and physical properties of the self-assembled structures are encoded in the corresponding characteristics of the building blocks, thereby offering the potential to rationally design materials with properties that are tailored to specific applications.[1–3] However, the assembly process is often driven by a subtle interplay of multiple intermolecular forces such as electrostatics, hydrogen bonding, hydrophobic, and solvent interactions. Control and rational design considerations are thus based on a thorough understanding of these fundamental driving interactions.

R. Mizuta, J. M. Devos, M. Oliva, M. Gray, J. Webster, D. Munnur, E. Mossou, R. Schweins, M. Haertlein, V. T. Forsyth
Institut Laue Langevin
71 Avenue des Martyrs, 38000 Grenoble, France
E-mail: rm832@cam.ac.uk

R. Mizuta, T. Narayanan, M. Gray, J. Webster, D. Munnur, E. Mitchell
European Synchrotron Radiation Facility
71 Avenue des Martyrs, 38000 Grenoble, France mitchell@esrf.fr

W.-L. Ling
Université Grenoble Alpes
CEA
CNRS
IBS
38000 Grenoble, France

A. Round
European Molecular Biology Laboratory
71 Avenue des Martyrs, 38000 Grenoble, France

D. Munnur, S. Neidle
School of Pharmacy
University College London
Brunswick Square, WC1N 1AX London, UK

E. Mossou, V. T. Forsyth
Faculty of Natural Sciences & Institute for Science and Technology in Medicine
Keele University
ST5 5BG Staffordshire, UK

A. Farahat
Department of Pharmaceutical Organic Chemistry
Faculty of Pharmacy
Mansoura University
Mansoura, Egypt

D. W. Boykin, W. D. Wilson
Department of Chemistry
Georgia State University
Atlanta, GA 30303, USA

P. Rannou
Université Grenoble Alpes
CNRS
CEA
INAC-SyMMES
38000 Grenoble, France

DOI: 10.1002/masy.201800243

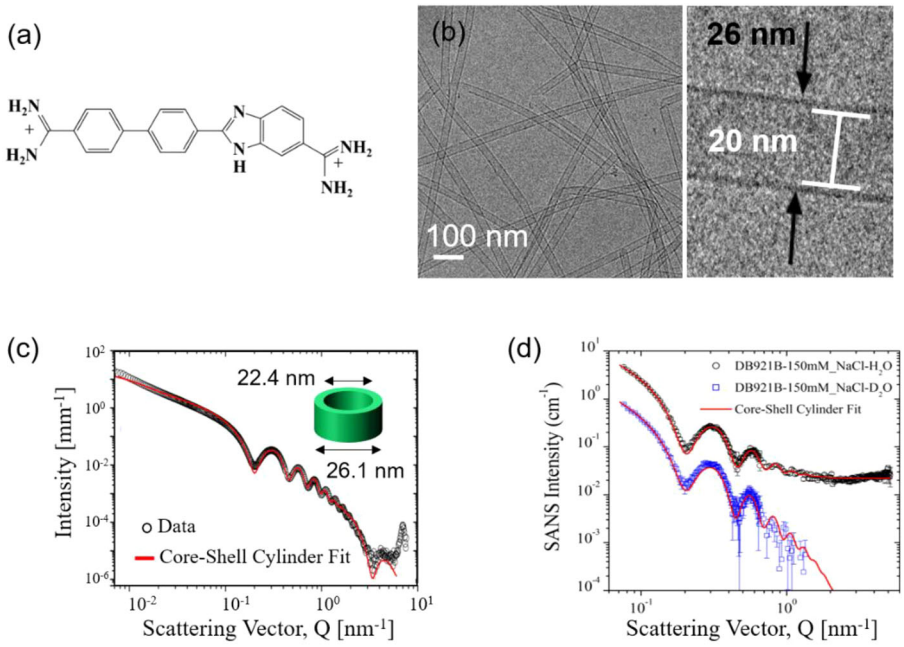

Figure 1. a) The chemical structure of a DB921 molecule, b) Cryo-TEM images of fully assembled DB921 nanotubes in NaCl, with an enlarged image of the nanotube cross section to indicate the estimated dimensions from TEM image analysis. c) SAXS data (ID02, ESRF) recorded from the fully assembled DB921 nanotubes in 150 mM NaCl, fitted with a hollow core-shell cylinder form factor. The cross-sectional dimensions obtained from the fit are illustrated in the inset figure. d) SANS data (Instrument D11, ILL) recorded from fully assembled DB921 nanotubes in 150 mM NaCl for H_2O (black) and D_2O (blue), fit with a core-shell cylinder form factor. Reproduced with permission.[4]

We have recently reported a novel supramolecular nanotube system formed by a heterocyclic cationic molecule, DB921 (**Figure 1**(a)).[4] This structural characterization work exploited small-angle X-ray and neutron scattering (SAXS and SANS), along with cryo-transmission electron microscopy, and indicates a hierarchical assembly mechanism via helical intermediates that is triggered by the addition of specific alkali halide salts. It is proposed that the primary driving interactions for the assembly are ionic interactions and the formation of aromatic π-π stacking interactions. Importantly, it is found that the alkali halide provides a convenient handle for modulating key properties of the system. The time-resolved SAXS studies highlight a critical anion concentration above which the rate of self-assembly is greatly enhanced. The alteration of the halide anion from chloride to bromide results in a clear change in nanotube diameter.

2. Experimental Results

2.1. Structural Characterization: DB921 Nanotubes in NaCl

DB921 nanotubes were assembled in the laboratories of ILL's Sciences Group.[5] They were formed by mixing a saturated aqueous solution of approximately 12 mM DB921 (including 8% (v/v) of dimethyl sulphoxide (DMSO)) with an equal volume of an aqueous solution of alkali halide at room temperature. Unless stated otherwise, a 300 mM alkali halide solution was employed, such that the final solution in which the nanotubes were formed contained 150 mM salt, 4% DMSO (v/v), and aqueous DB921 of approximately 6 mM concentration. It is noted that DB921 was supplied in powder form with an acetate counterion, and therefore all DB921 nanotube solutions of a given DB921 concentration will also contain an equivalent concentration of the acetate counterion.

The morphology of assembled DB921 nanotubes in NaCl was studied using solution-state small-angle X-ray scattering (SAXS) and neutron scattering (SANS), performed on the BM29, ID02 beamlines at the ESRF, and instrument D11 at the ILL, respectively.[6–9] Complementary cryo-transmission electron microscopy (TEM) of the assembled nanotubes was also performed to provide direct visualization of the nanotubes. As shown in the TEM images in Figure 1(b), the nanotubes are characterized by varying lengths that reach into the microns. In contrast, their cross-sectional diameters appear nearly monodisperse, yielding approximate values for inner and outer diameters of 20 and 26 nm respectively.

As shown in Figure 1(c), the 1-D high-resolution SAXS profile (ID02, ESRF) from fully assembled nanotubes shows numerous oscillations that can be modelled using a hollow core-shell cylinder form factor of uniform scattering length density.[10] Fitting the data using the software SASView yielded inner and outer nanotube diameters of 22.4 and 26.1 nm respectively, in close agreement with the values obtained from cryo-TEM. Similar values were found according to SANS (D11, ILL), yielding inner diameters (22.4 nm and 23.0 nm) and outer diameters (26.2 nm and 26.8 nm) for nanotubes in H_2O and D_2O solution, respectively, shown in Figure 1(d).

It is worth noting that the corresponding wall thickness of the nanotube (1.85 nm) closely matches the calculated length of a

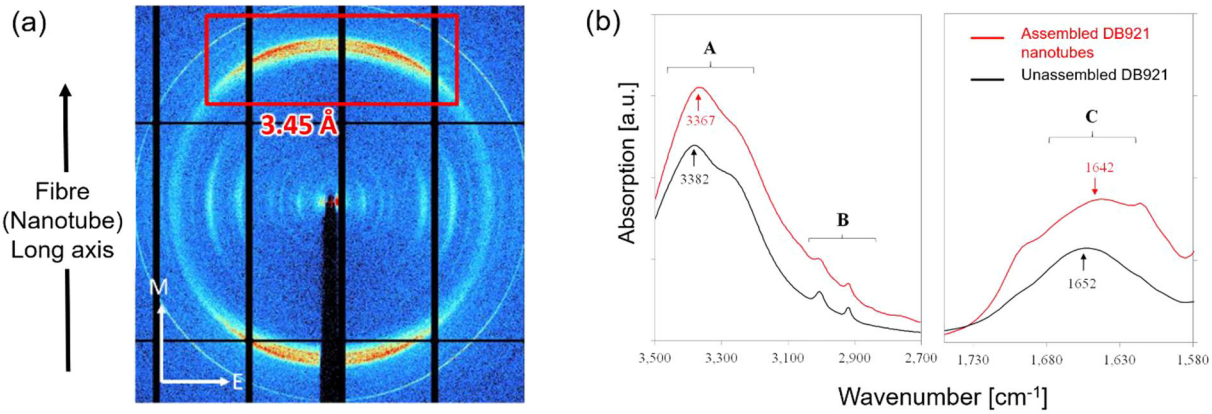

Figure 2. a) X-ray diffraction from fibres of partially aligned nanotubes (ID23-2 beamline, ESRF), where the nanotube long axis is aligned vertically along the meridional (M) axis. The red box indicates reflections at 3.45 Å corresponding to π-stacking. Reproduced with permission.[4] (b) FTIR spectra from unassembled DB921 (powder) and assembled nanotubes (dried), with N–H stretching (A), aromatic C–H stretching (B) and N–H bending (C) modes indicated.

single DB921 molecule along its long axis (1.92 nm), suggesting that the wall consists of a single layer of DB921 molecules. It is also noted that the sharp peak observed at approximately 7 nm^{-1} in Figure 1(c) is attributed to the periodicity of the DB921 molecules in the plane normal to the nanotube long axis, according to the proposed molecular model illustrated in ref. [4].

Given that nanotube formation was not observed in the absence of salt, the primary interaction that drives the self-assembly process is understood to be electrostatic by nature. However, it is believed that secondary non-bonding interactions may also contribute to dictate the assembled morphology. X-ray diffraction pattern from fibers of partially aligned nanotubes (**Figure 2**(a), taken on the ID23-2 beamline, ESRF) also exhibit prominent scattering peaks at 3.45 Å. This periodicity is consistent with typical aromatic π–π stacking arrangements.[11] Fiber samples of nanotubes were formed by suspending a droplet of aqueous nanotube solution between two rods and pulling the rods slowly apart as the droplet dried, allowing shear forces to induce molecular alignment. The fact that the aromatic stacking peak occurs on the meridian (the direction of the fiber axis) of the fiber diffraction pattern suggests that the π-stacking direction is parallel to the nanotube axis. Conversely, the diffraction peaks that lie on the equator of the pattern reflect features in the cross-sectional plane of the nanotube. In particular, the peaks found near to the center of the pattern in Figure 2(a) are equivalent to the peaks at approximately 7 nm^{-1} in Figure 1(c). In addition to π–π interactions, the Fourier transform infrared (FTIR) spectra obtained from unassembled DB921 powder and dried DB921 nanotubes exhibit small but noticeable differences. As shown in Figure 2(b), peaks found in the regions indicated by A and C are identified as N–H stretching and bending modes respectively, and are attributed to N–H bonds of the terminal amidinium groups and central benzimidazole group. These modes are both found shifted to lower wavenumbers upon formation of the nanotubes; it is assumed that this arises from a slight weakening of the N–H bonds that are associated with weak inter-DB921 hydrogen bonding interactions. For reference, it is noted that the aromatic stretching C–H modes identified as region B remain unchanged, reflecting the absence of hydrogen bonding associated with these groups.

2.2. Assembly Mechanism: DB921 Nanotubes in NaCl

In order to understand the self-assembly mechanism and kinetics of DB921, time-resolved (TR) studies were performed using joint SAXS and negative stain TEM imaging. In the case of TR-SAXS (BM29, ESRF), nanotubes were assembled with NaCl concentrations ranging from 30 mM to 150 mM to study the kinetic effect of increasing salt concentration on the assembly. For nanotubes assembling at a given NaCl concentration, multiple SAXS measurements were obtained over time to yield the time-evolution of the SAXS curves. From these studies, it was firstly found that a threshold NaCl concentration of ≈60 mM exists, below which the characteristic SAXS oscillations of the nanotubes do not appear over the experimental timescale of several hours (**Figure 3**(a)). It is important to note that such low NaCl concentrations may not necessarily preclude self-assembly altogether, but rather induce the process over significantly longer timescales (e.g. days). Above ≈60 mM, nanotube assembly may be confirmed by the emergence of characteristic SAXS oscillations over time, as illustrated in Figure 3(b) for 70 mM NaCl. In particular, two time regimes are noted: an initial induction period τ_i, that characterises a delay time before SAXS oscillations may be observed, followed by a growth period τ_g, during which the SAXS oscillations appear and evolve.

By taking the integral of SAXS intensity with scattering vector as a function of time, the induction time may be obtained according to the Avrami equation for growth kinetics.[4,12]

Figure 3(d) illustrates how the induction time varies with NaCl concentration; importantly, this shows that increasing salt concentration 60 mM and up to 100 mM dramatically shortens this induction period, and results in more rapid assembly. This may be rationalized in terms of the dicationic nature of the DB921 molecule in which the anions of the prevailing salt solution neutralize the positive charges on the terminal amidinium groups. Thus higher salt concentrations reduce

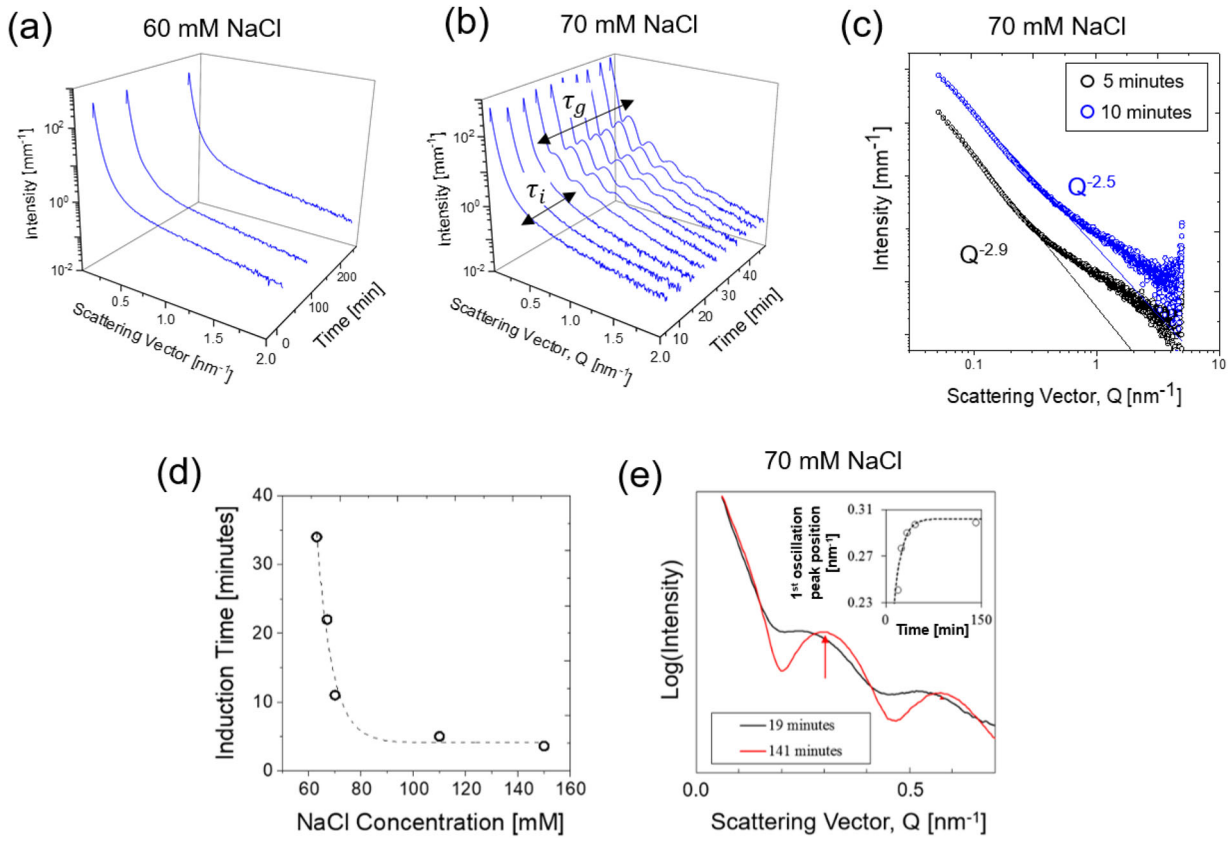

Figure 3. Time-resolved SAXS spectra (BM29, ESRF) at (a) 60 mM NaCl, exhibiting no nanotubes after ≈4 h, (b) 70 mM NaCl, illustrating nanotube formation in under 30 min. τ_i and τ_g indicate the induction and growth time respectively. (c) SAXS curves on a log-log plot for 70 mM NaCl after 5 min (black) and 10 min (blue) of assembly time. The curves are both fitted with a power-law fit shown by the solid lines, with the corresponding power-law relation shown. Note: the curves have been vertically displaced for visual clarity. (d) The variation of induction time with NaCl concentration, as calculated using the Avrami equation for growth kinetics, and (e) the shifting of nanotube SAXS curves to higher Q with increasing growth time at 70 mM NaCl. The inset shows the shift of the maximum of the first oscillation to higher Q with time. Reproduced with permission.[4]

the electrostatic repulsion between a larger number of DB921 molecules, facilitating more rapid self-assembly. The significance of the anion (and not the cation) of the salt is further corroborated by our systematic study of alternative salts, as explained in section 2.3. In contrast, Figure 3(e) shows that during the growth period, here illustrated for 70 mM NaCl, the maxima and minima of the SAXS curves are found to shift to higher scattering vectors. This is shown in detail in the inset of Figure 3(e), in which the position of the first oscillation maximum (shown by the red arrow in Figure 3(e)) is plotted over time in order to illustrate a shift from approximately 0.24 nm^{-1} to 0.29 nm^{-1}. With reference to the hollow core-shell cylinder form factor, such a shift suggests a decrease in cross-sectional diameter of the nanotubes.

The origin of the two time regimes may be understood from the TR-TEM shown in **Figure 4**, which illustrates that the nanotube assembly proceeds hierarchically via multiple intermediate structures. The assembly was followed for nanotube assembly in 4.5 mM DB921 and 60 mM NaCl to achieve slow assembly over 48 h and therefore improved ease of imaging. Within less than 1 h, short filaments with lengths of 2–5 nm emerge (Figure 4(a)). These subsequently evolve to longer fibrils (Figure 4(b)). Following 24 h of incubation, such ribbons appear to pack laterally into ribbons as shown in Figure 4(c), with the inset illustrating the splitting of the ends of the ribbons into individual fibrils. Finally, after 48 h, the ribbons proceed to form nanotubes via a helical winding process, illustrated for two different nanotubes in Figure 4(d). Importantly, it is assumed here that the assembly process and the observed intermediates remain unchanged at this lower DB921 concentration as compared with the ≈6 mM DB921 concentration employed in the TR-SAXS. Furthermore, TR-TEM was only performed for one NaCl concentration, and thus a similar assumption is made concerning the validity of the hierarchical assembly of intermediates across all tested NaCl concentrations during TR-SAXS.

With regards to the TR-SAXS, the characteristic SAXS oscillations of these nanotubes only emerge upon formation of hollow core-shell cylindrical structures. Therefore, the initial induction period is attributed to the time taken for the assembly to proceed up to the formation of ribbons, prior to their helical winding into nanotubes. During this induction period, the

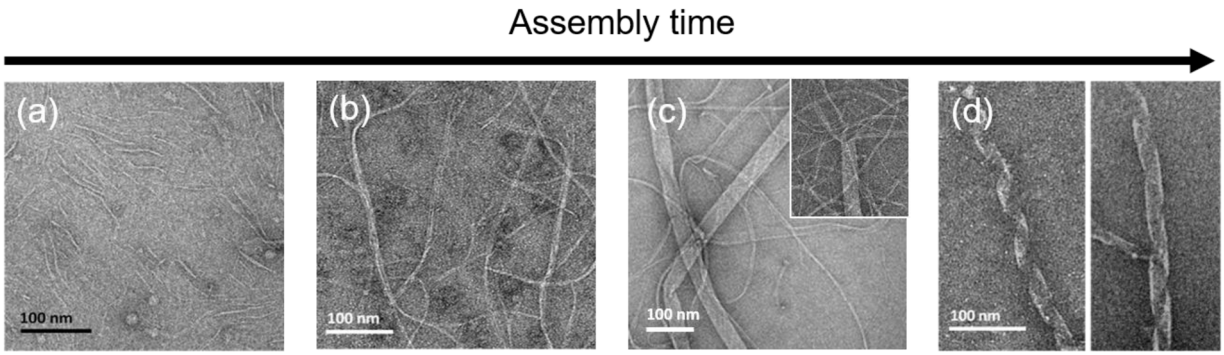

Figure 4. Time-resolved negative stain EM images taken during nanotube assembly with 4.5 mM DB921 in 60 mM NaCl, illustrating the hierarchical intermediates starting with (a) short fibrils, (b) long fibrils, (c) ribbons, and finally (d) ribbons helically winding into nanotubes. Reproduced with permission.[4]

scattering intensity $I(Q)$ follows an approximate power-law with scattering vector Q according to $I \propto Q^{-n}$ for low scattering vectors. This is illustrated in Figure 3(c), where the SAXS curves recorded from DB921 nanotubes in 70 mM NaCl after 5 and 10 min have been fitted using power-law relationships of $Q^{-2.5}$ and $Q^{-2.9}$, respectively. Deviations from this power law at higher scattering vectors are likely to arise from deficiencies in background subtraction (remaining DB921 molecules and salt in the solution). For an ideal system of dilute ribbons, the corresponding scattering is expected to follow a power law with $n = 2$.[13] The larger exponents found for the present system, along with their different values at these two times, are perhaps indicative of the multiple structural moieties (incomplete ribbons, curled ribbons, partially formed nanotubes) that are simultaneously present and evolving in solution.

In contrast, the growth period reflects the final helical winding step to complete nanotubes. With reference to the shifting of SAXS curves as described in Figure 3(e), it is important to note that the total scattering arises from a population of ribbons in which there is a distribution of ribbons at different stages of this helical winding process. Therefore, the peak shift to higher scattering vector reflects an increasing population of nanotubes that have formed from loosely wound helices to more tightly coiled nanotubes, leading to an apparent decrease in the cross-section. With reference to previous literature, such a hierarchical self-assembly via the helical winding of ribbon intermediates has also been observed in many systems, in particular the highly monodisperse nanotubes formed by lithocholic bile acid (LCA) studied by Terech et al.[14–16] Notably, the LCA nanotube system exhibits remarkably similar time-dependence of SAXS during nanotube formation, including the shifting of oscillations to higher scattering vector over time. This effect which is similarly attributed to the tightening of loose cylindrical structures into nanotubes of smaller diameter.[15]

2.3. Nanotube Assembly in Different Salts

In our previous report, the assembly of DB921 in different alkali halide (AX) salts was tested, whereby both the alkali metal cation (A) and halide anion (X) were systematically varied.[4] While varying the metal cation yielded no change in the assembly behavior (for A = Li, Na, K and X = Cl), **Figure 5**(a) illustrates that varying the halide anion significantly affects the assembly (X = F, Cl, Br, I). Notably, nanotube assembly occurred for chloride and bromide ions while no assembly was observed for fluoride and iodide anions. In addition, the nanotubes formed in chloride or

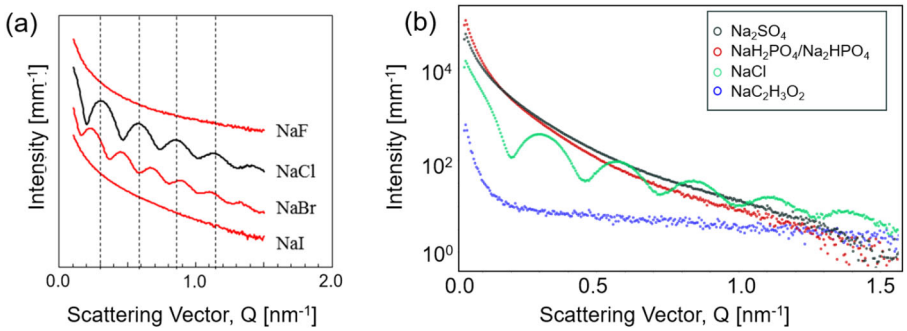

Figure 5. SAXS spectra (BM29, ESRF) of DB921 assembly in 150 mM salt for (a) different alkali halides, with the halide anion varied, and (b) for alternative inorganic anions, namely SO_4^{2-} (black), $C_2H_3O_2^-$ (blue) and $H_2PO_4^-/HPO_4^{2-}$ (red), compared to the fully formed nanotubes in NaCl (green). In all cases, a Na^+ counterion was used. In (a), SAXS curves are vertically translated in intensity for visual clarity. In (b), SAXS intensities were measured after one day of assembly, but characteristic oscillations were not observed for the new anions tested.

bromide ions exhibited different cross-sectional diameter as shown by the different maxima and minima positions in SAXS profile and TEM imaging. Indeed, fitting of the SAXS data recorded from bromide nanotubes with the same core-shell cylinder form factor (as described in ref. [4]), yields inner and outer diameters of 27.8 and 32.0 nm, respectively, that differ significantly from the chloride nanotubes. In contrast it is noted that the wall thickness in the bromide nanotubes (2.1 nm) does not significantly increase from that observed for the case of chloride nanotubes (1.9 nm), further supporting the proposal that the wall thickness is determined by the DB921 molecular length.

These results indicate that the choice of anion is critical in determining whether or not the assembly proceeds and also the final nanotube morphology. This opens up the possibility of tuning the physical properties of the nanotubes. In order to investigate this further, preliminary experiments using alternative anions have been conducted recently using SAXS. The salts tested were Na_2SO_4, $NaC_2H_3O_2$, and a solution of NaH_2PO_4/Na_2HPO_4 at pH 7. The DB921 nanotube samples were prepared as previously described via a two-fold dilution, adding a saturated DB921 solution (at a concentration close to 12 mM) to 300 mM of the salt and the solution was kept in the dark at 4 °C. The SAXS measurements were carried out one day after the samples were prepared on the BM29 beamline at ESRF, with each sample held at 20 °C. Figure 5(b) shows the SAXS curves from DB921 in Na_2SO_4 (black), $NaC_2H_3O_2$ (blue), and NaH_2PO_4/Na_2HPO_4 (red) after buffer subtraction. As can be seen, none of these newly investigated salts formed any regular nanotubes such as the ones we have seen for NaBr or NaCl (green, Figure 5(a)) under the conditions tested, further highlighting the elegant selectivity of the nanotube assembly for the nature of the anion. In particular, it is noted that in contrast to the solely monovalent halide anions that were previously studied, the anions of such salts include both monovalent anions ($C_2H_3O_2-$, H_2PO_4-) and divalent anions (SO_4^{2-}, HPO_4^{2-}).

3. Conclusion

In conclusion, a novel self-assembling nanotube system is presented, whereby DB921 molecules are found to self-assemble in salt solution. The study has investigated both the fundamental assembly process and the experimental parameters that influence it. The system is of fundamental value since it offers a platform for understanding self-assembling systems in the context of the various non-bonding interactions that dictate the assembly. The DB921 nanotube system is found to be governed by a complex interaction between salt anion and DB921. While electrostatic effects are likely to be an important contributor, the absence of self-assembly for anions other than Cl^- and Br^- suggests other competing effects that are not fully understood at this stage. Additional interactions between DB921 molecules themselves including aromatic π-stacking may also contribute.

The system is also extremely promising for potential applications, given the opportunities for rational control of the assembly. The time-resolved SAXS studies indicate that by simply varying the salt concentration, it is possible to alter the speed of assembly. In addition, our preliminary studies of different anions have indicated that the nanotube morphology may also be tuned by suitable selection of the salt. Combined with the fact that assembly proceeds in a hierarchical manner that culminates with the helical winding of ribbons into nanotubes, the system may be very promising as an encapsulating vessel for applications such as drug delivery.

Acknowledgements

The authors gratefully acknowledge the ESRF and ILL for the support of R.M., M.G., and J.W. during placements from Bath University (UK) to the EPN Campus (Grenoble, France). The authors acknowledge ESRF and ILL for access to X-ray and neutron scattering facilities. Much of the work was carried using the laboratory facilities of ILL's Life Sciences group – initially funded through EPSRC awards to V.T.F. (grants EP/C015452/1, GR/R99393/01) for the creation of the Deuteration Laboratory (D-Lab). In particular, they thank beamline scientist Mark Tully (BM29, BioSAXS) for his assistance with the most recent acquisition of preliminary SAXS data. This work benefited from the use of the SasView programme, originally developed under NSF award DMR-0520547. SasView contains code developed with funding from the European Union's Horizon 2020 research and innovation programme under the SINE2020 project, grant agreement no. 654000. This work used the platforms of the Grenoble Instruct Centre (ISBG: UMS 3518 CNRS-CEA-UJF-EMBL) with support from FRISBI (ANR-10-INSB-05-02) and GRAL (ANR-10-LABX-49-01) within the Grenoble Partnership for Structural Biology (PSB). The electron microscope facility is supported by the Rhône-Alpes Region, the Fondation Recherche Medicale (FRM), the fonds FEDER, the Centre National de la Recherche Scientifique (CNRS), the CEA, the University of Grenoble, EMBL, and the GIS-Infrastructures en Biologie Santé et Agronomie (IBISA). This research was supported, in part, by a US NIH grant (Grant No. GM111749) to W.D.W. and D.W.B.

Keywords

nanotubes, self-assembly, small-angle X-ray scattering, transmission electron microscopy

[1] J. Li, C. Fan, H. Pei, J. Shi, Q. Huang, *Adv. Mater.* **2013**, *25*, 4386.
[2] G. A. Ozin, K. Hou, B. V. Lotsch, L. Cademartiri, D. P. Puzzo, F. Scotognella, A. Ghadimi, J. Thompson, *Mater. Today* **2009**, *12*, 12.
[3] W. Childers, A. K. Mehta, T. Q. Bui, Y. Liang, D. G. Lynn, *Molecular Self Assembly: Advances and Applications*, Pan Stanford Publishing, Singapore **2013**.
[4] R. Mizuta, J. M. Devos, J. Webster, W. L. Ling, T. Narayanan, A. Round, D. Munnur, E. Mossou, A. A. Farhat, D. W. Boykin, W. D. Wilson, S. Neidle, R. Schweins, P. Rannou, M. Haertlein, V. T. Forsyth, E. P. Mitchell, *Nanoscale* **2018**, *10*, 5550.
[5] M. Haertlein, M. Moulin, J. M. Devos, V. Laux, O. Dunne, V. T. Forsyth, *Methods Enzymol.* **2016**, *566*, 113.
[6] P. Pernot, A. Round, R. Barrett, A. De Maria Antolinos, A. Gobbo, E. Gordon, J. Huet, J. Kieffer, M. Lentini, M. Mattenet, C. Morawe, C. Mueller-Dieckmann, S. Ohlsson, W. Schmid, J. Surr, P. Theveneau, L. Zerrad, S. McSweeney, *J. Synchrotron. Radiat.* **2013**, *20*, 660.
[7] M. E. Brennich, J. Kieffer, G. Bonamis, A. De Maria Antolinos, S. Hutin, P. Pernot, A. Round, *Acta Crystallogr. Sec. D: Struct. Biol.* **2016**, *D71*, 67.
[8] T. Narayanan, M. Sztucki, P. Van Vaerenbergh, J. Léonardon, J. Gorini, L. Claustre, F. Sever, J. Morse, P. Boesecke, *J. Appl. Cryst.* **2018**, *51*, 1511.

[9] P. Lindner, R. Schweins, *Neutron News* **2010**, *21*, 15.
[10] A. Guinier, G. Fournet, *Small-Angle Scattering of X-Rays*, John Wiley & Sons, Inc., New York **1955**.
[11] J. P. Hill, W. Jin, A. Kosaka, T. Fukushima, H. Ichihara, T. Shimomura, K. Ito, T. Hashizume, N. Ishii, T. Aida, *Science* **2004**, *304*, 1481.
[12] M. J. Avrami, *J. Chem. Phys.* **1939**, *7*, 1103.
[13] I. W. Hamley, *Macromolecules* **2008**, *41*, 8948.
[14] P. Terech, A. de Geyer, B. Struth, Y. Talmon, *Adv. Mater.* **2002**, *14*, 495.
[15] B. Jean, L. Oss-Ronen, P. Terech, Y. Talmon, *Adv. Mater.* **2005**, *17*, 728.
[16] P. Terech, B. Jean, F. Ne, *Adv. Mater.* **2006**, *18*, 1571.